

# Gravitational waves from axisymmetric rotating stellar core collapse to a neutron star in full general relativity

Masaru Shibata and Yu-ichirou Sekiguchi

*Graduate School of Arts and Sciences, University of Tokyo, Tokyo, 153-8902, Japan*

## Abstract

Axisymmetric numerical simulations of rotating stellar core collapse to a neutron star are performed in the framework of full general relativity. The so-called Cartoon method, in which the Einstein field equations are solved in the Cartesian coordinates and the axisymmetric condition is imposed around the  $y = 0$  plane, is adopted. The hydrodynamic equations are solved in the cylindrical coordinates (on the  $y = 0$  plane in the Cartesian coordinates) using a high-resolution shock-capturing scheme with the maximum grid size (2500, 2500). A parametric equation of state is adopted to model collapsing stellar cores and neutron stars following Dimmelmeier et al. It is found that the evolution of central density during the collapse, bounce, and formation of protoneutron stars agree well with those in the work of Dimmelmeier et al. in which an approximate general relativistic formulation is adopted. This indicates that such approximation is appropriate for following axisymmetric stellar core collapses and subsequent formation of protoneutron stars. Gravitational waves are computed using a quadrupole formula. It is found that the waveforms are qualitatively in good agreement with those by Dimmelmeier et al. However, quantitatively, two waveforms do not agree well. Possible

reasons for the disagreement are discussed.

04.25.Dm, 04.30.-w, 04.40.Dg

## I. INTRODUCTION

Rotating stellar core collapse is among the most promising sources of gravitational waves. To date, there has been no systematic work for computation of the collapse to a neutron star and of emitted gravitational waves in full general relativity (but see [1]). Gravitational waves associated with the formation of rotating neutron stars have been widely computed in the Newtonian gravity [2–9] or in an approximate general relativistic gravity [10] using the so-called conformal flatness approximation (or Isenberg-Wilson-Mathews approximation [11]). As indicated in [10], the general relativistic effects modify the dynamics of the collapse and corresponding gravitational waveforms significantly. This implies that simulation in full general relativity is the best approach for accurate computation of gravitational waves.

During the stellar core collapse to a neutron star, the characteristic radius changes from initial stellar core radius  $\sim 2000$  km to neutron star radius  $\sim 10$  km. Adopting a uniform and fixed grid with a grid spacing as  $\sim 1$  km, the required grid number for the simulation is more than 2000 for one direction. With current computational resources, it is very difficult to take such a huge number of grid points in three-dimensional simulations. If the progenitor of the neutron star is not very rapidly rotating, nonaxisymmetric instabilities will not set in and the collapse will proceed in an axisymmetric manner. By restricting our attention to axisymmetric spacetimes, the grid resolution can be improved significantly for a given computational resource. Thus, as a first step, it is better to perform axisymmetric simulations than to do nonaxisymmetric ones for a well-resolved and convergent computation of the collapse, the bounce, and corresponding gravitational waveforms, focusing only on the moderately rapid rotation case.

In this paper, we study gravitational waves from rotating stellar core collapses to a neutron star assuming the axial symmetry. Dynamics of the collapse is followed by fully general relativistic simulation. Gravitational waves are approximately computed using a quadrupole formula adopted and tested in [12]. Necessity of adopting quadrupole formulas arises from the fact that the amplitude of gravitational waves is too small ( $< 10^{-5}$  in the

local wave zone) to accurately extract the waveforms from raw data sets of metric. Although exact gravitational waveforms cannot be computed, the quadrupole formula is a useful tool for approximate computation of gravitational waves associated with matter motion such as oscillations of neutron stars as indicated in [12].

Recently, gravitational waves from axisymmetric rotating stellar core collapses have been extensively computed in a relativistic manner by Dimmelmeier et al. [10]. As mentioned above, they determine the gravitational fields adopting an approximate formulation of the Einstein equation. The approximation is likely to be applicable to a moderately relativistic and stationary spacetime such as that for a rapidly rotating neutron star [13]. However, no one has clarified whether this is the case for dynamical spacetimes. To confirm that their treatment is indeed appropriate, it is necessary to compare their solutions with fully general relativistic ones for a calibration. One of the purposes in this paper is to examine whether the numerical solution for the stellar core collapse computed in [10] is a well approximated one for a fully general relativistic solution.

In [10], gravitational waveforms were computed in terms of a quadrupole formula. In general relativity, there is no unique definition of the quadrupole moment, nor is the quadrupole formula, for axisymmetric dynamical spacetimes. Accuracy of gravitational waveforms depends on the choice of the quadrupole formula and the gauge conditions. Thus, to know how accurately the approximate gravitational waveforms can be computed by the chosen quadrupole formula, a calibration is required by comparing the resulting waveforms with those computed from the metric as we did in [12]. Unfortunately, such calibration is not possible in [10] since they adopted an approximate general relativistic formulation for the gravitational field in which the metric does not carry any information of gravitational waves. Consequently, it is not clear whether the quadrupole formula they adopted can actually yield accurate approximate gravitational waveforms and how large the magnitude of the error is. On the other hand, in the previous paper [12], we did such a calibration for a quadrupole formula which is different from that in [10], and showed it possible to compute gravitational waves from oscillating and rapidly rotating neutron stars of high values of compactness

fairly accurately, besides possible systematic errors for the amplitude due to neglecting post-Newtonian corrections. Computing gravitational waveforms by the calibrated quadrupole formula and comparing the results with the previous ones, we estimate how accurate the waveforms computed in [10].

This paper is organized as follows. In Sec. II, our numerical implementations for general relativistic simulation in axial symmetry are briefly reviewed. In Sec. III, the initial condition and computational setting are described. Sec. IV presents the numerical results. Sec. V is devoted to a summary. Throughout this paper, we adopt the geometrical units in which  $G = c = 1$  where  $G$  and  $c$  are the gravitational constant and the speed of light, respectively.

## II. NUMERICAL IMPLEMENTATION

### A. Summary of formulation

We perform fully general relativistic simulations for rotating stellar core collapse in axial symmetry using the same formulation as in [14], to which the reader may refer for details and basic equations. The fundamental variables for the hydrodynamics are

$\rho$ : rest mass density,

$\varepsilon$ : specific internal energy,

$P$ : pressure,

$u^\mu$ : four velocity,

$$v^i = \frac{dx^i}{dt} = \frac{u^i}{u^t}, \quad (1)$$

where subscripts  $i, j, k, \dots$  denote  $x, y$  and  $z$ , and  $\mu$  the spacetime components. As the variables to be evolved in the numerical simulations, we define a weighted density  $\rho_*(= \rho \alpha u^t e^{6\phi})$  and a weighted four-velocity  $\hat{u}_i [= (1 + \varepsilon + P/\rho)u_i]$ . From these variables, the total baryon rest-mass and angular momentum of system, which are conserved quantities in axisymmetric spacetimes, can be defined as

$$M_* = \int d^3x \rho_*, \quad (2)$$

$$J = \int d^3x \rho_* \hat{u}_\varphi. \quad (3)$$

General relativistic hydrodynamic equations are solved using a so-called high-resolution shock-capturing scheme [15,14] on the  $y = 0$  plane with the cylindrical coordinates  $(x, z)$  (in the Cartesian coordinates with  $y = 0$ ).

The fundamental variables for geometry are

$\alpha$ : lapse function,

$\beta^k$ : shift vector,

$\gamma_{ij}$ : metric in three dimensional spatial hypersurface,

$$\gamma = e^{12\phi} = \det(\gamma_{ij}),$$

$$\tilde{\gamma}_{ij} = e^{-4\phi} \gamma_{ij},$$

$K_{ij}$ : extrinsic curvature. (4)

We evolve  $\tilde{\gamma}_{ij}$ ,  $\phi$ ,  $\tilde{A}_{ij} \equiv e^{-4\phi}(K_{ij} - \gamma_{ij}K_k^k)$ , and trace of the extrinsic curvature  $K_k^k$  together with three auxiliary functions  $F_i \equiv \delta^{jk}\partial_j\tilde{\gamma}_{ik}$  with an unconstrained free evolution code as in [16,18–20,17,14].

The Einstein equations are solved in the Cartesian coordinates. To impose axisymmetric boundary conditions, the Cartoon method is used [22]: Assuming the reflection symmetry with respect to the equatorial plane, simulations are performed using a fixed uniform grid with the grid size  $N \times 3 \times N$  in  $(x, y, z)$  which covers a computational domain as  $0 \leq x \leq L$ ,  $0 \leq z \leq L$ , and  $-\Delta \leq y \leq \Delta$ . Here,  $N$  and  $L$  are constants and  $\Delta = L/N$ . In the Cartoon method, the axisymmetric boundary conditions are imposed at  $y = \pm\Delta$ .

As the time slice, we impose an ‘‘approximate’’ maximal slicing condition in which  $K_k^k \approx 0$  is required [16]. As the spatial gauge, we adopt a dynamical gauge condition [21] in which the equation for the shift vector is written as

$$\partial_t \beta^k = \tilde{\gamma}^{kl}(F_l + \Delta t \partial_t F_l), \quad (5)$$

where  $\Delta t$  denotes a timestep in numerical computation.

During the numerical simulations, violations of the Hamiltonian constraint and conservation of mass and angular momentum are monitored as code checks. Numerical results for several test calculations, including stability and collapse of nonrotating and rotating neutron stars, have been described in [14].

An outgoing wave boundary condition for  $F_i$ ,  $h_{ij}(= \tilde{\gamma}_{ij} - \delta_{ij})$ , and  $\tilde{A}_{ij}$  is imposed at the outer boundaries of the computational domain. The condition adopted is the same as that described in [20].  $K_k^k$  is set to be zero at the outer boundaries.

## B. Equations of state

A parametric equation of state is adopted following Müller and his collaborators [6,10]. In this equation of state, one assumes that the pressure consists of the sum of polytropic and thermal parts as

$$P = P_P + P_{\text{th}}. \quad (6)$$

The polytropic part is given by  $P_P = K_P(\rho)\rho^{\Gamma(\rho)}$  where  $K_P$  and  $\Gamma$  are not constants but functions of  $\rho$ . In this paper, we follow [10] for the choice of  $K_P(\rho)$  and  $\Gamma(\rho)$ : For the density smaller than the nuclear density which is defined as  $\rho_{\text{nuc}} \equiv 2 \times 10^{14} \text{ g/cm}^3$ ,  $\Gamma = \Gamma_1(=\text{const})$  is set to be  $\lesssim 4/3$ , and for  $\rho \geq \rho_{\text{nuc}}$ ,  $\Gamma = \Gamma_2(=\text{const}) \geq 2$ . Thus,

$$P_P = \begin{cases} K_1 \rho^{\Gamma_1}, & \rho \leq \rho_{\text{nuc}}, \\ K_2 \rho^{\Gamma_2}, & \rho \geq \rho_{\text{nuc}}, \end{cases} \quad (7)$$

where  $K_1$  and  $K_2$  are constants. Since  $P_P$  should be continuous, the relation,  $K_2 = K_1 \rho_{\text{nuc}}^{\Gamma_1 - \Gamma_2}$ , is required. Following [6,10], the value of  $K_1$  is fixed to  $5 \times 10^{14}$  cgs. With this choice, the polytropic part of the equation of state for  $\rho < \rho_{\text{nuc}}$ , in which the degenerate pressure of electrons is dominant, is approximated well. Since the specific internal energy should be continuous at  $\rho = \rho_{\text{nuc}}$ , the polytropic specific internal energy  $\varepsilon_P$  is defined as

$$\varepsilon_{\text{P}} = \begin{cases} \frac{K_1}{\Gamma_1 - 1} \rho^{\Gamma_1 - 1}, & \rho \leq \rho_{\text{nuc}}, \\ \frac{K_2}{\Gamma_2 - 1} \rho^{\Gamma_2 - 1} + \frac{(\Gamma_2 - \Gamma_1) K_1 \rho_{\text{nuc}}^{\Gamma_1 - 1}}{(\Gamma_1 - 1)(\Gamma_2 - 1)}, & \rho \geq \rho_{\text{nuc}}. \end{cases} \quad (8)$$

With this setting, a realistic equation of state for high-density, cold nuclear matter is mimicked.

The thermal part of the pressure  $P_{\text{th}}$  plays an important role in the case that shocks are generated.  $P_{\text{th}}$  is related to the thermal energy density  $\varepsilon_{\text{th}} \equiv \varepsilon - \varepsilon_{\text{P}}$  as

$$P_{\text{th}} = (\Gamma_{\text{th}} - 1) \rho \varepsilon_{\text{th}}. \quad (9)$$

Following [10], the value of  $\Gamma_{\text{th}}$ , which determines the strength of shocks, is chosen as 1.5 for most simulations in this paper. Extending the previous work [10], for a few models, we set  $\Gamma_{\text{th}} = 1.35$  or  $5/3$  to investigate the effect of the shock heating at the bounce phase and resulting gravitational waveforms.

Simulations are initiated in the following manner: First, equilibrium rotating stars with  $\Gamma = 4/3$  polytrope are given. Then, to induce the collapse, we slightly decrease the value of the adiabatic index from  $\Gamma = 4/3$  to  $\Gamma_1 < 4/3$ . The equilibrium states are computed with the polytropic equation of state as

$$P = K_0 \rho^{4/3}, \quad (10)$$

where following [10],  $K_0$  is set to be  $5 \times 10^{14} \text{ cm}^3/\text{s}^2/\text{gr}^{1/3}$ , with which a soft equation of state governed by the electron degenerate pressure is approximated well [23]. Here,  $K_0$  and  $K_1$  are related by  $K_1 = K_0 \rho_0^{4/3 - \Gamma_1}$  where we set  $\rho_0 = 1 \text{ g/cm}^3$ .

### C. Quadrupole formula

In the present work, gravitational waveforms are computed using a quadrupole formula [12]. In quadrupole formulas, gravitational waves at null infinity are calculated from

$$h_{ij} = P_i^k P_j^l \left( \frac{2}{r} \frac{d^2 I_{kl}}{dt^2} \right), \quad (11)$$



where  $I_{ij}$  and  $P_i{}^j = \delta_i{}^j - n_i n^j$  ( $n^i = x^i/r$ ) denote a tracefree quadrupole moment and the projection tensor. From this expression, the +-mode of gravitational waves with  $l = 2$  in axisymmetric spacetimes is written as

$$h_+^{\text{quad}} = \frac{\ddot{I}_{xx}(t_{\text{ret}}) - \ddot{I}_{zz}(t_{\text{ret}})}{r} \sin^2 \theta, \quad (12)$$

where  $I_{ij}$  denotes a quadrupole moment,  $\ddot{I}_{ij}$  its second time derivative, and  $t_{\text{ret}}$  a retarded time.

In fully general relativistic and dynamical spacetimes, there is no unique definition for the quadrupole moment and nor is for  $\ddot{I}_{ij}$ . Following a previous paper [12], we choose the simplest definition as

$$I_{ij} = \int \rho_* x^i x^j d^3x. \quad (13)$$

Then, using the continuity equation of the form

$$\partial_t \rho_* + \partial_i (\rho_* v^i) = 0, \quad (14)$$

the first time derivative can be written as

$$\dot{I}_{ij} = \int \rho_* (v^i x^j + x^i v^j) d^3x. \quad (15)$$

To compute  $\ddot{I}_{ij}$ , the finite differencing of the numerical result for  $\dot{I}_{ij}$  is carried out.

As indicated in [12], it is possible to compute gravitational waves from oscillating and rapidly rotating neutron stars of high values of compactness fairly accurately with the present choice of  $I_{ij}$ , besides possible systematic errors for the amplitude of order  $M/R$  or  $v^2/c^2$  where  $M$ ,  $R$ , and  $v$  denote the gravitational mass, the equatorial circumferential radius, and the radial velocity of the collapsing star and/or formed neutron stars. In stellar core collapses,  $v^2/c^2$  is at most  $\sim 0.1$ , and the outcomes are protoneutron stars of  $M/R \sim 0.1$ . Thus, it is likely that the wave amplitude is computed within  $\sim 10\%$  error. The wave phase will be computed very accurately as indicated in [12].

| Model | $\rho_c$ (g/cm <sup>3</sup> ) | $M_*(M_\odot)$ | $M(M_\odot)$ | $R$ (km) | $T/W$                 | $J/M^2$ | $\alpha_c$ | $\Omega_a$ (1/sec) | $\hat{A}$ |
|-------|-------------------------------|----------------|--------------|----------|-----------------------|---------|------------|--------------------|-----------|
| A     | $1.00 \times 10^{10}$         | 1.503          | 1.503        | 2267     | $8.91 \times 10^{-3}$ | 1.235   | 0.994      | 4.11               | $\infty$  |
| B     | $1.00 \times 10^{10}$         | 1.485          | 1.485        | 1576     | $5.00 \times 10^{-3}$ | 0.839   | 0.994      | 6.49               | 0.32      |
| C     | $1.00 \times 10^{10}$         | 1.488          | 1.488        | 1568     | $5.44 \times 10^{-3}$ | 0.841   | 0.994      | 8.45               | 1/4       |
| D     | $1.00 \times 10^{10}$         | 1.500          | 1.500        | 1571     | $1.01 \times 10^{-2}$ | 1.146   | 0.994      | 11.6               | 1/4       |

TABLE I. Central density, baryon rest-mass, ADM mass, equatorial circumferential radius, ratio of the rotational kinetic energy to the potential energy, non-dimensional angular momentum parameter, central value of the lapse function, angular velocity at the rotational axis, and  $\hat{A}$  of rotating stars chosen as initial conditions for stellar core collapse simulations.

### III. INITIAL CONDITION AND COMPUTATIONAL SETTING

Rotating stellar core in equilibrium with the  $\Gamma = 4/3$  polytropic equation of state [see Eq.(10)] is given as the initial condition for simulations. Following [10], the central density is chosen as  $\rho_c = 10^{10}$  g/cm<sup>3</sup> irrespective of the velocity profile.

The velocity profiles of equilibrium rotating stellar cores are given according to a popular relation [24,25]

$$u^t u_\varphi = \varpi_d^2 (\Omega_a - \Omega), \quad (16)$$

where  $\Omega_a$  denotes the angular velocity along the rotational axis, and  $\varpi_d$  is a constant. In the Newtonian limit, the rotational profile is written as

$$\Omega = \Omega_a \frac{\varpi_d^2}{\varpi^2 + \varpi_d^2}. \quad (17)$$

Thus,  $\varpi_d$  indicates the steepness of differential rotation. In this paper, we pick up the rigidly rotating case in which  $\varpi_d \rightarrow \infty$  (referred to as model A) and differentially rotating cases with  $\hat{A} \equiv \varpi_d/R_e = 0.32$  (referred to as model B) and 1/4 (referred to as models C and D), where  $R_e$  is the coordinate radius at an equatorial surface. In the rigidly rotating case, we

chose the axial ratio of polar radius to equatorial radius as  $2/3$ . With this choice, the angular velocity at the equatorial stellar surface is nearly equal to the Keplerian velocity. Namely, for the rigidly rotating case, a rapidly rotating initial condition with nearly maximum angular velocity is chosen. In the differentially rotating case, we chose stars of ratio of the rotational kinetic energy  $T$  to the gravitational potential energy  $W$  as  $\sim 0.005$  and  $\sim 0.01$  where

$$T = \frac{1}{2} \int d^3x \rho_* \hat{u}_\varphi \Omega, \quad (18)$$

$$W = \int d^3x \rho_* (1 + \varepsilon) - M + T. \quad (19)$$

Here,  $W$  is defined to be positive. In Table I, several quantities for the models adopted in the present numerical computation are summarized.

For the differentially rotating case with a small value of  $\hat{A} (< 1)$ , it is possible to make equilibrium states with  $T/W \gg 0.01$ . With such an initial condition, the collapsing stellar core often forms a differentially rotating star of a highly nonspherical shape and of a high value of  $T/W$  [7]. It is also known that rapidly rotating neutron stars of a high degree of differential rotation is dynamically unstable against nonaxisymmetric deformation (e.g., [26] and references therein). To simulate the collapse with a high initial value of  $T/W$ , a nonaxisymmetric simulation will be necessary. Since our attention here is restricted to the axisymmetric case, we do not choose such initial conditions.

Simulations are performed for four initial conditions listed in Table I. Models A and B are almost the same initial conditions as models A1B3 and A3B2 in [10]. (Note that the value of  $A$  for model B is  $\approx 5 \times 10^2$  km which is approximately equal to that for model A3B2 in [10].) Careful comparison of present numerical results with those in [10] is carried out using these two models. A variety of values of  $\Gamma_1$ ,  $\Gamma_2$ , and  $\Gamma_{\text{th}}$  are adopted to investigate the dependence of numerical results on the equations of state:  $\Gamma_1$  is chosen as 1.28, 1.30, 1.31, and 1.32,  $\Gamma_2$  as 2 and 2.5, and  $\Gamma_{\text{th}}$  as 1.35, 1.5, and  $5/3$ . The selected sets are listed in Table II.

During the collapse, the central density increases from  $10^{10}$  g/cm<sup>3</sup> to  $\sim 5 \times 10^{14}$  g/cm<sup>3</sup>. This implies that the characteristic length scale of the system varies by a factor of  $\sim 100$ .

| Model | $\Gamma_1$ | $\Gamma_2$ | $\Gamma_{\text{th}}$ |
|-------|------------|------------|----------------------|
| A1    | 1.32       | 2.5        | 1.5                  |
| A2    | 1.31       | 2.5        | 1.5                  |
| A3    | 1.28       | 2.5        | 1.5                  |
| A4    | 1.32       | 2.5        | 1.35                 |
| A5    | 1.32       | 2.5        | 5/3                  |
| A6    | 1.32       | 2.0        | 1.5                  |
| B1    | 1.32       | 2.5        | 1.5                  |
| B2    | 1.30       | 2.5        | 1.5                  |
| C1    | 1.32       | 2.5        | 1.5                  |
| C2    | 1.30       | 2.5        | 1.5                  |
| C3    | 1.32       | 2.0        | 1.5                  |
| C4    | 1.32       | 2.5        | 1.35                 |
| D     | 1.32       | 2.5        | 1.5                  |

TABLE II. Selected sets of  $\Gamma_1$ ,  $\Gamma_2$ , and  $\Gamma_{\text{th}}$ .

One of the computational issues in a stellar core collapse simulation is to guarantee numerical accuracy against the significant change of the characteristic length scale. In the early phase of the collapse (infall phase; see Sec. IV A) in which it proceeds in a nearly homologous manner, we may follow the collapse with a relatively small number of grid points by moving the outer boundary inward while decreasing the grid spacing, without increasing the grid number by a large factor. As the collapse proceeds, the central region shrinks more rapidly than the outer region does and, hence, a better grid resolution is necessary to accurately follow such a rapid collapse in the central region. On the other hand, the location of the outer boundaries cannot be changed by a large factor to avoid discarding the matter in the outer envelopes.

| Model             | $\Delta x$ (initial) | $L$ (initial) | $\Delta x$ (final) | $L$ (final) |
|-------------------|----------------------|---------------|--------------------|-------------|
| A                 | 3.775                | 2265          | 0.4719             | 1180        |
| A(low resolution) | 6.292                | 2643          | 0.7865             | 1337        |
| B                 | 2.601                | 1613          | 0.3251             | 813         |
| B(low resolution) | 3.902                | 1639          | 0.4877             | 829         |
| C                 | 2.613                | 1568          | 0.3267             | 817         |
| D                 | 2.617                | 1570          | 0.3271             | 818         |

TABLE III. The initial and final grid spacings and location of the outer boundaries along the  $x$  and  $z$  axes for models A–D. The unit is kilometer.

To compute such a collapse accurately while saving the CPU time efficiently, a regridding technique as described in [27] is adopted. The regridding is carried out whenever the characteristic radius of the collapsing star decreases by a factor of a few. At each regridding, the grid spacing is decreased by a factor of 2. All the quantities in the new grid are calculated using the cubic interpolation. To avoid discarding the matter in the outer region, we also increase the grid number at the regridding, keeping a rule that the discarded baryon rest-mass has to be less than 3% of the total.

Specifically,  $N$  and  $L$  in the present work are chosen in the following manner. First, we define a relativistic gravitational potential  $\Phi_c \equiv 1 - \alpha_c$  ( $\Phi_c > 0$ ), which is  $\approx 0.006$  at  $t = 0$  for all the models chosen in this work. Since  $\Phi_c$  is approximately proportional to  $M/R$ ,  $\Phi_c^{-1}$  can be used as a measure of the characteristic length scale for the regridding. From  $t = 0$  to the time at which  $\Phi_c = 0.025$ , we set  $N = 620$ . Note that the equatorial radius is initially covered by 600 grid points. At  $\Phi_c = 0.025$ , the characteristic stellar radius becomes approximately one fourth of the initial value. Then, the first regridding is performed; the grid spacing is changed to the half of the previous one and the grid number is increased to  $N = 1020$ . Subsequently, the value of  $N$  is chosen in the following manner; for  $0.025 \leq \Phi_c \leq 0.05$ , we

set  $N = 1020$ ; for  $0.05 \leq \Phi_c \leq 0.1$ , we set  $N = 1700$ ; and for  $0.1 \leq \Phi_c$ , we set  $N = 2500$  and keep this number until the termination of the simulations since the maximum value of  $\Phi_c$  is at most 0.25. In this treatment, the total discarded fraction of the baryon rest-mass which is located outside new regridded domains is  $\lesssim 3\%$ .

To check the convergence of numerical results, we also perform a few simulations using a low grid resolution (cf. Table III). In this case, the value of  $N$  is changed as follows: for  $\Phi_c \leq 0.025$ ,  $N = 420$ ; for  $0.025 \leq \Phi_c \leq 0.05$ ,  $N = 820$ ; for  $0.05 \leq \Phi_c \leq 0.1$ ,  $N = 1300$ ; and for  $0.1 \leq \Phi_c$ ,  $N = 1700$ .

Simulations for each model with the higher grid resolution are performed for 60000–80000 time steps. The required CPU time for one model is about 40–70 hours using 8 processors of FACOM VPP 5000 at the data processing center of National Astronomical Observatory of Japan.

## IV. NUMERICAL RESULTS

### A. Dynamics of the collapse

#### 1. General feature

Figures 1–4 show the evolution of the central density (hereafter  $\rho_c$ ) and the central value of the lapse function (hereafter  $\alpha_c$ ) for models A – D. Figures 5 and 6 are snapshots of the density contour curves and the velocity vectors of  $(v^x, v^z)$  on the  $y = 0$  plane for models A1 and C1 at selected time slices around which shocks are formed.

As described in [10], rotating stellar core collapses can be divided into three phases. The first one is the infall phase in which the core collapse proceeds from the onset of the gravitational instability triggered by the sudden softening of the equation of state due to the reduction of the adiabatic index. During this phase, the central density (the central value of the lapse function) monotonically increases (decreases) until it reaches the nuclear density or the centrifugal force becomes strong enough to halt the collapse. The inner part of the

core, which collapses nearly homologously, constitutes the inner core. The duration of the infall phase in the present work is between about 30 and 70 msec depending mainly on the value of  $\Gamma_1$  (for the smaller value of  $\Gamma_1$ , the duration is shorter) as shown in [10]. We note that the dynamical time at  $t = 0$  defined by  $\rho_c^{-1/2}$  is  $\approx 38.7$  msec. Thus, the duration may be written as  $0.8\text{--}1.8 \rho_c^{-1/2}$ .

The second one is the bounce phase which sets in when the densities around the central part exceed the nuclear density  $\rho_{\text{nuc}}$ , or when centrifugal forces, which become stronger as the collapse proceeds due to angular momentum conservation, begin to dominate over gravitational attraction force. At this phase, the inner core decelerates infall in about a few msec ( $\sim 10\rho_{\text{nuc}}^{-1/2}$ ). Because of its large inertia and large kinetic energy due to the infall, the inner core does not settle down to a stationary state immediately but overshoots and bounces back, forming shocks at the outer edge of the inner core.

The third one is the ring-down phase or the re-expansion phase. If the centrifugal force is sufficiently small at the time that the density of the inner core exceeds the nuclear density, the bounce occurs when the central density reaches  $\sim 2\text{--}3\rho_{\text{nuc}}$  due to a sudden stiffening of the equation of state. In this case, the inner core quasiradially oscillates for about 10 msec and then settles down to a quasistationary state. In the outer region, on the other hand, shock waves propagate outward sweeping materials which infall from outer envelopes.

If the angular momentum in the inner region is sufficiently large, the collapse is halted by the centrifugal force, not by the sudden stiffening of the equation of state. In this case, the stellar core does not settle down to a quasistationary state. Instead, it rebounds due to the centrifugal force and expands to be of a subnuclear density. After the maximum expansion is reached, the core starts collapsing again. It repeats the bounce, the expansion, and the collapse for many times. During each bounce, shocks are formed at the outer region of the core and the oscillation amplitude is damped gradually due to the shock dissipation.

For models A–C, the centrifugal force is not strong enough to halt the collapse and, hence, a protoneutron star of the central density larger than the nuclear density is formed irrespective of the values of  $\Gamma_1$ ,  $\Gamma_2$ , and  $\Gamma_{\text{th}}$  (see Figs. 1–3). On the other hand, for model

D, the angular momentum is large enough to halt the collapse and to prevent the inner core being compact. As a result, the outcome is an oscillating star of a subnuclear density (see Fig. 4). Since the amplitude of the oscillation decreases gradually, it will settle to a rotating star of subnuclear density eventually. The adiabatic constant of this star is  $\approx \Gamma_1$  that is smaller than  $4/3$  which is the well-known critical value against gravitational collapse for spherical stars, and 1.329 which is an approximate critical value for rigidly rotating stars [28]. This indicates that the centrifugal force by a rapid and differential rotation plays an essential role for the stabilization against gravitational collapse. According to [29], the criterion of the stability for slowly rotating stars is given by

$$Q_c \equiv 3\Gamma_1 - 4 - 2\frac{T}{W}(3\Gamma_1 - 5) - k\frac{M}{R} > 0, \quad (20)$$

where  $k$  is a constant which is  $\approx 6.75$  for  $n = 3$  and  $T/W = 0$  [30]. For the Newtonian polytropes with  $n \approx 3$ , the stellar radius is given by

$$R \approx 2.35 \left(\frac{M}{\rho_c}\right)^{1/3} \approx 73 \text{ km} \left(\frac{M}{1.5M_\odot}\right)^{1/3} \left(\frac{\rho_c}{10^{14} \text{ g/cm}^3}\right)^{-1/3}. \quad (21)$$

Thus,  $M/R$  will be  $\sim 0.03$  for  $\rho_c \sim 10^{14} \text{ g/cm}^3$ . The value of  $T/W$  for dynamical stars is not exactly defined in general relativity, but assuming that it approximately increases as  $1/R \propto 1 - \alpha_c$  for a fixed value of  $M$ , we can infer that the value of  $T/W$  would be  $\sim 0.15$ – $0.2$  for  $\alpha_c \sim 0.9$  and  $k = 6.75$ . Therefore,  $Q_c$  would be  $\sim 0.1$ – $0.2$ , and, hence, the rotating star would satisfy the stability condition against gravitational collapse. On the other hand, the expected value of  $T/W$  is so large that the formed differentially rotating star may be unstable against a nonaxisymmetric deformation [26]. This suggests that to clarify the fate of this star, it would be necessary to perform a nonaxisymmetric simulation [18]. However, such a simulation is beyond scope of this paper and, hence, particular attentions are paid only to models A–C in this paper.

As Figs. 1(a) and 2(a) indicate, the evolution of the central density and the central value of the lapse function depends strongly on the value of  $\Gamma_1$ . For the smaller value of  $\Gamma_1$ , the depleted pressure at  $t = 0$  is larger. As a result, the collapse is accelerated more



and the elapsed time in the infall phase is shorter. Also, since the depleted fraction of the pressure is larger in the central region than in the outer region, the collapse in the central region proceeds more rapidly. This results in a less coherent collapse for the smaller value of  $\Gamma_1$ . This effect makes the mass of a protoneutron star at its formation smaller and is reflected in the value of  $\alpha_c$  in the ring-down phase which depends on the compactness of the protoneutron star. On the other hand, the final value of  $\rho_c$  depends only weakly on the value of  $\Gamma_1$ . This indicates that for the smaller value of  $\Gamma_1$ , the formed protoneutron star has a more centrally concentrated structure.

In Figs. 1(b) and 2(b), the evolution of the central density and the central value of the lapse function for different values of  $\Gamma_{\text{th}}$  with fixed values of  $\Gamma_1(= 1.32)$  and  $\Gamma_2(= 2.5)$  is compared. Recall that the value of  $\Gamma_{\text{th}}$  determines the strength of shocks at the bounce and at their subsequent propagation. Thus, the results here show that a moderate change of the value of  $\Gamma_{\text{th}}$  from 1.35 to 5/3 weakly modifies the evolution of the formed protoneutron stars. For the smaller value of  $\Gamma_{\text{th}}$ , the final value of the central density (central lapse) is larger (smaller). This is simply because the amount of matter that accretes to the protoneutron star increases and, hence, the compactness increases with the decrease of the value of  $\Gamma_{\text{th}}$ . For the larger value of  $\Gamma_{\text{th}}$ , the oscillation amplitude of  $\rho_c$  is larger. This is due to the fact that the stronger shocks result in the larger amplitude of the oscillation of the core.

In Figs. 1(c) and 2(b), the evolution of the central density and the central value of the lapse function is compared for different values of  $\Gamma_2$  with fixed values of  $\Gamma_1(= 1.32)$  and  $\Gamma_{\text{th}}(= 1.5)$ . [Compare the solid and dotted-dashed curves in Fig. 2(b).] Since the equation of state for a protoneutron star is stiffer for the larger value of  $\Gamma_2$ , the maximum density at the bounce, the final relaxed value of  $\rho_c$ , and the compactness of the quasistationary neutron star are smaller. Since the infall proceeds deeply inside the core, the amplitude of the oscillation for the central density in the ring-down phase is larger for the smaller value of  $\Gamma_2$ .

Figure 3 shows the evolution of the central density and the central value of the lapse function (a) for models B1 and C1 and (b) for models B2 and C2. The values of  $\Gamma_1$ ,  $\Gamma_2$ , and

$\Gamma_{\text{th}}$  are identical between models B1 and C1 and between models B2 and C2. Furthermore, the values of  $T/W$  for the initial condition are approximately equal. Therefore, the difference of the numerical results comes from the angular velocity profile of the initial conditions. Figure 3 indicates that the degree of differential rotation at  $t = 0$  is reflected significantly in the oscillation and evolution of the formed protoneutron stars. The quantitative differences are summarized as follows: (i) the time at the bounce  $t_b$  for models C1 and C2 is slightly larger than that for models B1 and B2, respectively; (ii) the maximum value of the central density for models C1 and C2 is slightly smaller than that for models B1 and B2, respectively; (iii) the amplitude of the oscillation of the central density and central value of the lapse function in the ring-down phase is larger for models C1 and C2. The results (i) and (ii) are simply due to the fact that the centrifugal force around the central region for models C1 and C2 is slightly larger and plays a stronger role for halting the collapse. The result (iii) indicates that the small increase of the angular velocity around the central region in the initial condition can significantly modify the evolution of the central density. All the results (i)–(iii) also show that the oscillation of the central density of the formed protoneutron stars depends strongly on the initial angular velocity profile.

Effects of differential rotation of the initial condition are also reflected significantly in the shape of the formed protoneutron stars. In the collapse of a rigidly rotating progenitor, the formed protoneutron star has a slightly nonspherical shape (see Fig. 5). On the other hand, in the collapse of a differentially rotating progenitor, a protoneutron star of a flattened and nonspherical shape is the outcome (see Fig. 6). This difference results from the fact that the inner region is more rapidly rotating in the case of the differentially rotating progenitor. It is worthy to note that the value of  $T/W$  for model A is about 1.6 times as large as that for model C. However, the angular velocity at the rotational axis for model A is about half of that for model C. Thus,  $T/W$  alone is not a good indicator for measuring the significance of the centrifugal force in rotating stellar core collapses (nor is the nondimensional angular momentum parameter  $J/M^2$ ). Obviously, the local distribution of the angular momentum plays a more important role for determining the shapes of the formed protoneutron star and

shocks.

Convergence of the numerical results is achieved well in the present computation. In Figs. 1(d), 3(a), and 3(b), we show the numerical results with a low grid resolution for models A1, B1, and B2 (dotted curves). It is found that the evolution of the central density and the central lapse in the low-resolution simulation agrees with that in the high-resolution one within a small error (except for the very late time for which the numerical error seems to be accumulated for the low-resolution simulation). This indicates that the grid resolutions adopted in the present numerical simulation are fine enough to yield a convergent numerical result.

## *2. Comparison with a previous work*

Here, we compare the numerical results for models A1, A2, A3, B1 and B2 with those for models A1B3G2, A1B3G3, A1B3G5, A3B2G2, and A3B2G4 in [10], respectively. For these models, both groups adopt the almost identical initial conditions.

Table IV shows the time at a maximum density achieved, the maximum density, and the maximum amplitude of gravitational waves for the numerical results computed by two groups. In Fig. 7, we also compare the evolution of the central density. It is found that the numerical results by two groups agree within a small error both for models A and B. Only for model B1, the time at the maximum density achieved slightly disagrees with that for A3B2G2 by  $\sim 0.3$  msec, but besides this disagreement, the shape of  $\rho_c$  as a function of time agrees well each other even in this case. Recall that in [10], the conformal flatness approximation to the Einstein equation is adopted while our results are fully general relativistic. This indicates that the conformal flatness approximation is a good approximate formulation of general relativity for computing axisymmetric rotating stellar core collapses to a neutron star.

In a precise comparison, the following small systematic disagreements between two results should be also addressed: (i) the maximum density achieved in our results is slightly larger

for model A and slightly smaller for model B; (ii) the time at the maximum density is slightly delayed in our results, and this tendency is stronger for the larger value of  $\Gamma_1$  (i.e., for the longer infall time); (iii) for the larger value of  $\Gamma_1$ , the central density in the relaxed final stage is slightly smaller in our results.

It is difficult to specify the particular reason for these disagreements. There are several plausible candidates. First, computational settings are different between two groups. In our simulation, we adopted a uniform grid changing the grid spacing and grid number, while in [10], 200 radial grid points with the logarithmic grid spacing were taken throughout the simulation. In our case, the grid spacing is smaller than 0.5 km in the bounce and ring-down phases, although it is larger than 0.5 km in the infall phase. On the other hand, the minimum grid spacing is about 0.5 km in [10] for all the phases. These differences may yield the disagreements. Actually, we find that varying the grid resolution results in a small change of the time at the maximum density achieved for models A1 and B1 [cf. Figs. 1(d) and 3(a)]. Secondly, the slicing condition is slightly different between two groups. In [10], the maximal slicing condition,  $K_k^k = 0$ , was adopted, while in our numerical simulation, the condition is only approximately satisfied [16]: The equations  $K_k^k = 0 = \partial_t K_k^k$  lead to an elliptic-type equation for  $\alpha$ . In the exact maximal slicing condition, this equation is iteratively solved until a convergence is achieved. In our case, we stop the iteration before the complete convergence is achieved to save the computational time. Thus,  $K_k^k \approx 0$ . This difference may result in a systematic deviation of the coordinate time at the maximum density. Thirdly, the initial conditions adopted by two groups are not completely identical, since the equilibrium rotating stars for the initial conditions are computed with different numerical implementations. The values of  $T/W$  and  $\hat{A}$  may well have disagreement of magnitude  $\lesssim 1\%$ . This may affect the subsequent numerical evolution slightly.

On the other hand, the difference of the adopted formulations for the gravitational field is unlikely to be the reason for the disagreement. This is because the deviation of the conformal metric  $\tilde{\gamma}_{ij}$  from  $\delta_{ij}$  is very small (typical absolute magnitude is of order  $\sim 10^{-3}$  for each component) in our numerical results. Therefore, we infer that the magnitude of

| Model  | $t_b$ | $\rho_{\max}$ (g/cm <sup>3</sup> ) | $(rh_+)_{\max}$ (cm) |
|--------|-------|------------------------------------|----------------------|
| A1     | 69.5  | 4.12                               | 561                  |
| A1B3G2 | 69.5  | 4.02                               | 469                  |
| A2     | 48.7  | 4.28                               | 215                  |
| A1B3G3 | 48.6  | 4.23                               | 180                  |
| A3     | 30.3  | 4.98                               | 32.7                 |
| A1B3G5 | 30.2  | 4.55                               | 33.9                 |
| B1     | 69.8  | 3.93                               | 731                  |
| A3B2G2 | 69.5  | 4.10                               | 596                  |
| B2     | 39.3  | 3.92                               | 182                  |
| A3B2G4 | 39.3  | 4.05                               | 141                  |

TABLE IV. Comparison between the present (upper) and previous numerical results by Dimmelmeier et al. (lower). The time at bounce, the maximum density achieved, and the maximum amplitude of gravitational waves are shown for two numerical results.

the systematic error due to the conformally flatness approximation seems to be smaller than that due to other reasons.

## B. Gravitational waveforms

### 1. General feature

Gravitational waveforms are computed in terms of the quadrupole formula described in Sec. II C. Since fully general relativistic simulations are performed, gravitational waves should be computed from the metric in a wave zone. However, we have found that it is not possible, since the amplitude is smaller than the numerical noise. An estimate by the quadrupole formula indicates that the maximum amplitude of gravitational waves is smaller

than  $10^{-5}$  in the local wave zone for  $r \sim \lambda$  where  $\lambda$  denotes the wave length which is typically several hundred km.

As illustrated in a previous paper [12], approximate gravitational waveforms can be computed in terms of a quadrupole formula for highly relativistic, highly oscillating, and rapidly rotating neutron stars. In rotating stellar core collapses to a neutron star, gravitational waves are dominantly emitted during the bounce and ring-down phases. Such gravitational waves are excited by oscillations of a formed protoneutron star. Thus, it is likely that the present approach can yield high-quality approximate gravitational waveforms besides possible underestimation of the amplitude by  $\sim 10\%$  due to absence of higher general relativistic corrections.

Figures 8(a)–(d) show gravitational waveforms for model A with various sets of  $\Gamma_1$ ,  $\Gamma_2$ , and  $\Gamma_{\text{th}}$ . The waveforms for models A1, A2, A4, A5, and A6 are classified into type I according to Dimmelmeier et al. [10]. Properties of the type I gravitational waveforms can be summarized as follows: During the infall phase, a precursor whose amplitude and characteristic frequency increase monotonically with time is emitted due to the infall and the flattening of the rotating core. The duration of the infall phase is  $\gtrsim 40$  msec and longer than a dynamical time scale defined at  $t = 0$  as  $\rho_c^{-1/2} \sim 40$  msec. In the bounce phase, spiky burst waves are emitted for a short time scale  $\sim 1$  msec, and the amplitude and the frequency of gravitational waves become maximum. In the ring-down phase, gravitational waves associated with several oscillation modes of a formed protoneutron star are emitted and its amplitude is gradually damped due to shock dissipation at the outer edge of the protoneutron star.

For model A3 [cf. Fig. 8(c)] for which the simulation is performed with a small value of  $\Gamma_1$  as 1.28, the waveforms are qualitatively different from those for others: A sharp and distinguishable peak is not found at the bounce. Soon after the precursor emitted during the infall phase, the ring-down waveforms appear to be excited. An outstanding feature is that the amplitude in this case is much smaller than that for  $\Gamma_1 = 1.31$  and 1.32 although the wave length is not significantly different from those for other models. According to [10],

this type of the waveforms is classified into type III.

In Fig. 8(a), the waveforms for models A1, A4, and A5 are presented. For these models, we adopt  $\Gamma_1 = 1.32$  and  $\Gamma_2 = 2.5$ , so that only the value of  $\Gamma_{\text{th}}$  is different. In the infall phase, the waveforms for three models are very similar. This is natural because as long as the density is smaller than  $\rho_{\text{nuc}}$ , the magnitude of  $P_{\text{th}}$  is much smaller than that of the cold part. Clear differences in the wave phase, wave length, and amplitude are observed in the bounce and ring-down phases. The reasons for them are explained as follows: The smaller magnitude of  $P_{\text{th}}$  results in the slightly shorter infall time as reflected in the time at which the amplitude becomes maximum. As a consequence, the difference of the wave phase is yielded. Stronger shock heating, which generates larger thermal energy, also results in smaller compactness of the formed protoneutron stars. This leads to the results that for the larger value of  $\Gamma_{\text{th}}$ , the gravitational wave length, which in general increases with the stellar radius for a given mass, becomes longer, and the amplitude, which is larger for stronger shock heating, is larger.

Slight change of the value of  $\Gamma_1$ , which determines the dynamics of the infall phase, significantly modifies gravitational waveforms. Comparison among Figs. 8(a)–(c) clarifies that with the decrease of the value of  $\Gamma_1$ , the amplitude of gravitational waves decreases systematically. The reason for this is explained as follows: For the smaller value of  $\Gamma_1$ , the central region collapses more rapidly than the outer region does. This results in a smaller core mass at the bounce for the smaller value of  $\Gamma_1$ . The amplitude of gravitational waves increases with the increase of the core mass for a fixed value of the density and, therefore, it is smaller for the smaller value of  $\Gamma_1$ .

In Fig. 8(d), we compare the waveforms of different values of  $\Gamma_2$  with fixed values of  $\Gamma_1$  and  $\Gamma_{\text{th}}$ . It is found that the difference of the waveforms between two models appears only in the bounce and ring-down phases. This is natural because the value of  $\Gamma_2$  does not affect the infall phase and mainly determines the equations of state and the radius (or compactness) of the formed protoneutron stars. Recall that the smaller value of  $\Gamma_2$  results in the larger compactness of the protoneutron star. This fact is reflected in slightly shorter wave length

and larger amplitude of gravitational waves in the ring-down phase for the smaller value of  $\Gamma_2$ .

Figure 9 displays gravitational waveforms for model C. As in the case of model A, the waveforms are divided into three parts (precursor, spike, and ring-down), but the qualitative feature of the ring-down waveforms between models A and C is different. For example, compare the waveforms for models A1 and C1 for which the values of  $\Gamma_1$ ,  $\Gamma_2$ , and  $\Gamma_{\text{th}}$  are identical. For model A1, the waveforms are modulated only in the early ring-down phase (e.g., for  $t \sim 70\text{--}73$  msec). In the late ring-down phase (e.g., for  $t \gtrsim 73$  msec for model A1), they are fairly periodic and appear to be composed mainly of one or two eigen oscillation modes of the formed protoneutron star. On the other hand, for model C1, the waveforms are not very periodic and highly modulated throughout the ring-down phase. In this case, several eigen modes of a formed protoneutron star appear to constitute gravitational waveforms. Such modulated waveforms are likely to be due to the fact that the formed protoneutron star is rapidly and differentially rotating and the oscillation modes are excited in a complicated manner at the bounce.

In Fig. 9(a), we compare the waveforms of different values of  $\Gamma_{\text{th}}$  with fixed values of  $\Gamma_1$  and  $\Gamma_2$ . As in Fig. 8(a), for the smaller value of  $\Gamma_{\text{th}}$ , the maximum amplitude is reached at an earlier time, the wave length during the bounce and ring-down phases is longer, and the amplitude is smaller. These are universal features independent of the initial rotational velocity profiles. However, in contrast to Fig. 8(a), the waveforms in the ring-down phase for models C1 and C4 are not very similar. Thus, small change of  $\Gamma_{\text{th}}$  from 1.35 to 1.5 significantly modifies the ring-down waveform in the case of differentially rotating initial velocity profiles.

In Fig. 9(b), we compare the waveforms of different values of  $\Gamma_2$  with fixed values of  $\Gamma_1$  and  $\Gamma_{\text{th}}$ . In contrast to Fig. 8(d), the maximum amplitude of gravitational waves is nearly identical for two models. This suggests that in halting the infall, the centrifugal forces may play an important role to hide the effects of the difference in the value of  $\Gamma_2$ . The difference of the ring-down waveforms between two models is qualitatively the same as that found in



Fig. 8(d): For the smaller value of  $\Gamma_2$ , the wave length and amplitude of gravitational waves in the ring-down phase are slightly shorter and larger, respectively.

In Fig. 9(c), the waveform for model C2 is displayed. This should be compared with the solid curve in Fig. 9(a) [or 9(b)] for model C1 of a different value of  $\Gamma_1$ . Comparison between two waveforms shows that with the decrease of the value of  $\Gamma_1$ , the wave amplitude at the bounce and ring-down phases decreases. This property agrees with that found for model A and is likely to be independent of the initial rotational velocity profiles.

To see the effect of the slight change of differential rotation parameter  $\hat{A}$ , we compare the waveforms of models B1 (solid curve) and C1 (dotted-dashed curve) in Fig. 9(d). Two waveforms are qualitatively similar, but for model C1 the amplitude is larger and the modulation of the amplitude is induced more. This illustrates that with a slight modification of the initial rotational velocity profile, the resulting gravitational waveforms are modified significantly.

Figure 10 shows the gravitational waveform for model D. In this model, the collapse does not lead to a quasistationary protoneutron star of  $\rho_c > \rho_{\text{nuc}}$ . Instead, a quasiradially oscillating star of subnuclear density is formed and, therefore, quasiperiodic waves of a long period  $\sim 10$  msec are emitted. According to [10], this is classified into the type II waveform.

Convergence of the numerical results appears to be achieved. In Fig. 11, we display the numerical results with high and low grid resolutions for models A1 and B1. The grid spacing in the low grid resolution is about 5/3 as large as that in the high case. It is found that the computed gravitational waveforms depend only weakly on the grid resolution in our choice of the grid spacing. We conclude that the grid resolution we choose in this work is fine enough to compute convergent gravitational waveforms.

## *2. Comparison with a previous work*

Here, we compare the gravitational waveforms computed in this paper with those in [10] for models A1, A2, A3, B1, and B2. Figures 12 and 13 show the gravitational waveforms

computed by us (solid curves) and by Dimmelmeier et al. [10] (dashed curves). It is found that the waveforms in the infall phase agree very well each other. In the bounce phase, on the other hand, the amplitude of our results is larger than that in [10] by  $\sim 20\%$  for models A1, A2, B1, and B2, although they still agree qualitatively. The disagreement is outstanding in the ring-down phase. The amplitudes of gravitational waves in the ring-down phase for models A1, A2, B1, and B2 are larger than those in [10] by a factor of  $\sim 2$ . Moreover, in our results, the oscillations with a nearly constant amplitude continue for several oscillation periods ( $\gtrsim 10$  msec). This is not the case in the results of [10] in which the amplitude is damped within several msec.

This would be partly due to the difference in the grid resolution or in the slicing condition adopted by two groups as mentioned in the previous section. However, the main reason is likely that quadrupole formulas adopted by two groups are not identical. In the quadrupole formula we adopt, a quadrupole moment is simply defined using a weighted rest-mass density  $\rho_*$  and then the second time derivative is taken with no approximation. In [10], on the other hand, the quadrupole moment is defined using  $\rho$  and, in addition, when taking the second time derivative, they discard higher relativistic terms keeping only the lowest order post-Newtonian terms.

This disagreement raises a question: what is a good quadrupole formula in general relativistic simulations? An excellent quadrupole formula should yield a high-quality approximate waveform for the true one computed from the metric in the wave zone. Thus, to answer the question, it is necessary to compare the gravitational waveforms computed by a quadrupole formula with those extracted from the metric. In [12], we calibrated the waveforms by performing simulations for highly relativistic, highly oscillating, and rapidly rotating neutron stars with  $M/R \sim 0.2$  and  $v/c \sim 0.3$  and found that our quadrupole formula yields well-approximated waveforms; the wave phases agree well with those computed from the metric and the wave amplitude is computed within an error of magnitude of  $O(M/R)$  or  $O(v^2/c^2)$ . We believe that the waveforms presented in this paper are well-approximated ones in phase and within  $\sim 10\%$  error in amplitude. On the other hand, the quadrupole

formula adopted in [10] has not been calibrated, since they adopted the conformal flatness approximation in which gravitational waves cannot be extracted from the metric. Thus, it is not clear how good their quadrupole formula is. Since the amplitudes computed by our quadrupole formula are underestimated by  $\sim 10\%$  and the amplitudes computed in [10] are smaller than ours, gravitational waveforms presented in [10] may contain an error of magnitude more than 10–20%.

## V. SUMMARY

We performed axisymmetric numerical simulations of rotating stellar core collapses to a neutron star in full general relativity, paying particular attention to gravitational waveforms and to comparison of our results with previous results [10]. The Einstein field equations are solved in the Cartesian coordinates imposing an axisymmetric condition by the Cartoon method [22]. The hydrodynamic equations are solved in the cylindrical coordinates (with the Cartesian coordinates restricting on the  $y = 0$  plane) using a high-resolution shock-capturing scheme with the maximum grid size (2500, 2500). A parametric equation of state is adopted to model collapsing stellar cores and formed protoneutron stars following Dimmelmeier et al. [10]. Gravitational waveforms are computed using a quadrupole formula proposed in [12].

We choose moderately rapidly rotating stars as the initial conditions for which the value of  $T/W$  is between 0.005 and 0.01. Simulations are performed changing three parameters ( $\Gamma_1$ ,  $\Gamma_2$ , and  $\Gamma_{\text{th}}$ ) which characterize the equation of state. The dynamics of the collapse depends on the three parameters as well as  $T/W$  and  $\hat{A}$  of the initial condition. The dependence of the evolution of the system and gravitational waveforms on these five parameters is studied. The value of  $\Gamma_1$  mainly determines the duration of the infall phase and the coherence of the early phase of the collapse. For the smaller value of  $\Gamma_1$ , the infall time becomes shorter and the collapse is accelerated more in the central region. This results in that the core mass at the bounce is smaller and that the magnitude of  $\Phi_c$  (which may be regarded as the depth of the gravitational potential) at the bounce is smaller for the smaller value of  $\Gamma_1$ . The

amplitude of gravitational waves becomes also smaller for the smaller value of  $\Gamma_1$ .

The value of  $\Gamma_2$  determines the equation of state for formed protoneutron stars. Thus, it does not affect the evolution during the infall phase. It determines the final value of the central density of the formed protoneutron star and the gravitational waveforms emitted during the ring-down phase in which the eigen oscillation modes of the protoneutron stars are excited. The value of  $\Gamma_{\text{th}}$  determines the strength of shock waves. We choose this value as 1.35, 1.5, and 5/3 extending the work by Dimmelmeier et al. [10]. It is found that for the smaller value of this parameter, the shock heating becomes weaker and the amplitude of gravitational waves smaller.

The values of  $T/W$  and  $\hat{A}$  play a significant role in determining the dynamics of collapse and the corresponding gravitational waveforms in particular in the bounce and ring-down phases. For the rigidly rotating case ( $\hat{A} \rightarrow \infty$ ), the maximum value of  $T/W$  is  $\approx 0.009$  which we choose in this paper. Even in this maximum case, the collapse leads to a neutron star irrespective of the values of  $\Gamma_1$ ,  $\Gamma_2$ , and  $\Gamma_{\text{th}}$ . This indicates that for rigidly rotating initial conditions, the neutron stars are formed soon after the collapse, irrespective of the angular velocity of the initial condition, with our choice of the equations of state. For the differentially rotating case with  $\hat{A} = 1/4$ , the collapse does not lead to a neutron star but an oscillating star of subnuclear density is formed for  $T/W \gtrsim 0.01$  since the centrifugal force is strong enough near the rotational axis. As shown in [10], more rapidly rotating initial conditions with  $T/W \gg 0.01$  may be constructed. For such high values of  $T/W$ , a neutron star will not be formed soon after the collapse.

With a slight change of  $\hat{A}$  from 0.25 to 0.32 for the initial condition, the angular velocity at the rotational axis is changed by a large factor even if  $T/W$  is approximately identical. As a result of this change, the subsequent evolution of the collapse and gravitational waveforms in the bounce and ring-down phases are modified significantly. This implies that the dynamics rotating stellar core collapses and the corresponding gravitational waveforms are sensitive not only to the equation of state but also to the initial angular velocity profile.

Several simulations are performed setting the same initial conditions as those adopted in

[10]. It is found that the dynamics of the collapse and the bounce for such initial conditions are very similar to those found in [10], in which an approximate general relativistic gravity (the conformal flatness approximation) is assumed. This indicates that such approximate relativistic formulation is appropriate for computing axisymmetric rotating stellar core collapses and the subsequent formation of protoneutron stars. (Note that this is the conclusion for the formation of neutron stars. This may not be the case for the black hole formation.)

Gravitational waveforms are compared with a previous result [10]. It is found that the waveforms are qualitatively in good agreement but not quantitatively with those in [10]. Either of two plausible elements could explain this disagreement. One is that the grid resolution and computational setting are different between two groups. This could modify the waveforms slightly. However, the main reason seems to be that the adopted quadrupole formulas by two groups are different. As mentioned in the previous section, there is no unique definition of the quadrupole formula for dynamical spacetimes in general relativity. This implies that when one attempts to use a quadrupole formula in a relativistic simulation, one needs to calibrate the formula in advance by performing a fully general relativistic simulation and by comparing the waveforms computed by the quadrupole formula with those computed from the metric. The quadrupole formula adopted in our study has been calibrated in simulations for highly relativistic, highly oscillating, and rapidly rotating neutron stars [12]. Thus, we believe that the quadrupole formula adopted in this paper is appropriate and that the numerical results presented here are approximate solutions of high quality.

In this paper, we have focused on the neutron star formation and on the comparison with a previous work [10]. If more massive progenitor is chosen as the initial condition, a black hole instead of a neutron star will be formed. Formation of black holes and corresponding gravitational waves have been studied by several groups [31,32,17]. However, the initial conditions in their previous works are not very realistic for modeling a rotating stellar core collapse in nature. Namely, the stellar core collapse to a black hole from a realistic initial condition in fully general relativistic simulation is an unsolved issue. We are currently

working in this subject and will present the numerical results in a subsequent paper.

### **Acknowledgments**

We thank Toni Font for discussion and careful reading of this manuscript, and Harald Dimmelmeier for comments. We also thank Harald Dimmelmeier, Toni Font, Jose-Maria Ibáñez, and Eward Müller for suggesting this work. Numerical computations were performed on the FACOM VPP5000 machine in the data processing center of National Astronomical Observatory of Japan. This work is in part supported by Japanese Monbu-Kagakusho Grants (Nos. 14047207, 15037204, and 15740142).

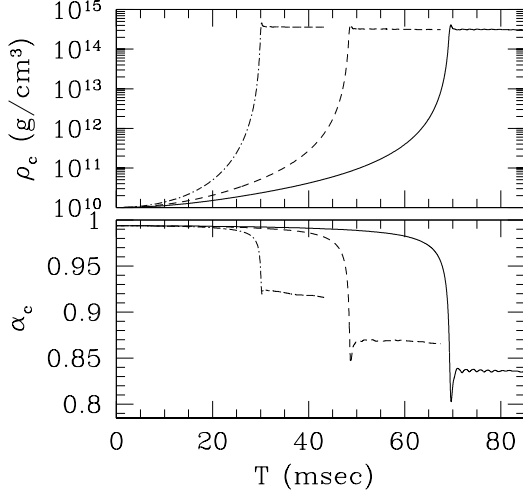
## REFERENCES

- [1] F. Siebel, J. A. Font, E. Müller, and P. Papadopoulos, *Phys. Rev. D* **67**, 124018 (2003).
- [2] L. S. Finn and C. R. Evans, *Astrophys. J.* **351**, 588 (1990).
- [3] R. Mönchmeyer, G. Schäfer, E. Müller and R. Kates, *Astron. and Astrophys.* **246**, 417 (1991). E. Müller, M. Rampp, R. Buras, H.-T. Janka, and D. H. Shoemaker, *astro-ph/0309833*.
- [4] S. Bonazzola and J.-A. Marck, *Astron. Astrophys.* **267**, 623 (1993).
- [5] S. Yamada and K. Sato, *Astrophys. J.* **434**, 268 (1994): **450**, 245 (1995): K. Kotake, S. Yamada, and K. Sato, *Phys. Rev. D* **68**, 044023 (2003).
- [6] T. Zwerger and E. Müller, *Astron. Astrophys.* **320**, 209 (1997).
- [7] M. Rampp, E. Müllelr and M. Ruffert, *Astron. Astrophys.* **332**, 969 (1998).
- [8] C. Fryer and A. Heger, *Astrophys. J.* **541**, 1033 (2000): C. Fryer, D. E. Holz and A. Heger, *Astrophys. J.* **565**, 430 (2002).
- [9] C. D. Ott, A. Burrows, E. Livne, and R. Walder, *astro-ph/0307472*.
- [10] H. Dimmelmeier, J. A. Font and E. Müller, *Astro. Astrophys.* **388**, 917 (2002); **393**, 523 (2002).
- [11] J. Isenberg and J. Nester, in *General Relativity and Gravitation* Vol.1, edited by A. Held, (Plenum Press, New York 1980); *Waveless Approximation Theories of Gravity*, preprint (1978), University of Maryland.
- [12] M. Shibata and Y. Sekiguchi, *Phys. Rev. D* **68**, 104020 (2003).
- [13] G. B. Cook, S. L. Shapiro, and S. A. Teukolsky, *Phys. Rev. D* **53**, 5533 (1996).
- [14] M. Shibata, *Phys. Rev. D* **67**, 024033 (2003).
- [15] J. A. Font, Living Review

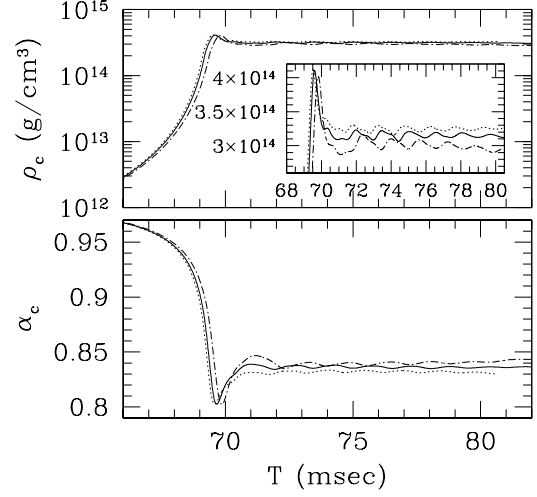
- Relativity **3**, 2, 2000 <http://www.livingreviews.org/Articles/Volume2/2000-2>font: F. Banyuls, J. A. Font, J.-Ma. Ibáñez, J. M. Martí, and J. A. Miralles, *Astrophys. J.* **476**, 221 (1997).
- [16] M. Shibata, *Prog. Theor. Phys.* **101**, 1199 (1999); *Phys. Rev. D* **60**, 104052 (1999).
- [17] M. Shibata, *Prog. Theor. Phys.* **104**, 325 (2000).
- [18] M. Shibata, T. W. Baumgarte and S. L. Shapiro, *Phys. Rev. D* **61**, 044012 (2000); *Astrophys. J.* **542**, 453 (2000).
- [19] M. Shibata and K. Uryū, *Phys. Rev. D* **61**, 064001 (2000): *Prog. Theor. Phys.* **107**, 265 (2002); M. Shibata, K. Taniguchi, and K. Uryū, *Phys. Rev. D* **68**, (2003).
- [20] M. Shibata and T. Nakamura, *Phys. Rev. D* **52**, 5428 (1995): In [16,18,19] and this paper, we adopt a formulation slightly modified from the original version presented in this reference.
- [21] M. Shibata, *Astrophys. J.* **595**, 992 (2003).
- [22] M. Alcubierre, S. Brandt, B. Brügmann, D. Holz, E. Seidel, R. Takahashi and J. Thornburg, *Int. J. Mod. Phys. D* **10**, 273 (2001).
- [23] For example, S. L. Shapiro and S. A. Teukolsky, *Black Holes, White Dwarfs, and Neutron Stars* (Wiley Interscience, New York, 1983).
- [24] See, e.g., H. Komatsu, Y. Eriguchi, and I. Hachisu, *Mon. Not. R. Astron. Soc.*, **237**, 355 (1989); **239**, 153 (1989).
- [25] See N. Stergioulas, *Living Rev. Relativ.*, **1**, 8 (1998) for a historical review about computation of relativistic rotating stars.
- [26] M. Shibata, S. Karino, and Y. Eriguchi, *Mon. Not. R. Astron. Soc.*, **334**, L27 (2002): **343**, 619 (2003).



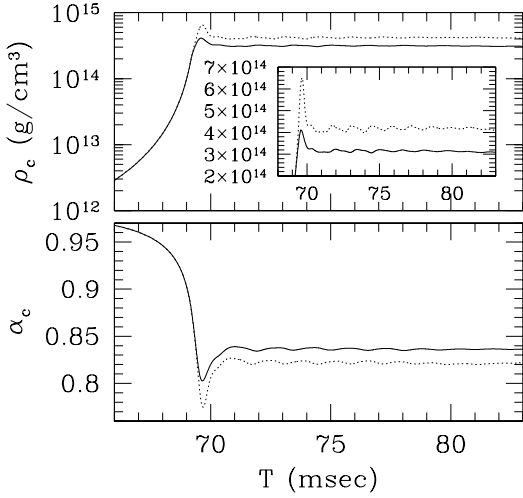
- [27] M. Shibata and S. L. Shapiro, *Astrophys. J. Lett.* **572**, L39 (2002).
- [28] M. Shibata, *Astrophys. J.* (2004), in press.
- [29] J.-L. Tassoul, *Theory of Rotating Stars* (Princeton University Press, Princeton, New Jersey, 1978).
- [30] S. Chandrasekhar, *Astrophys. J.* **140**, 417 (1964).
- [31] T. Nakamura, *Prog. Theor. Phys.* **65**, 1876 (1981); **70**, 1144 (1983).
- [32] R. F. Stark and T. Piran, *Phys. Rev. Lett.* **55**, 891 (1985); in *Dynamical Spacetimes and Numerical Relativity*, edited by J. M. Centrella (Cambridge University Press, Cambridge, England), p. 40.



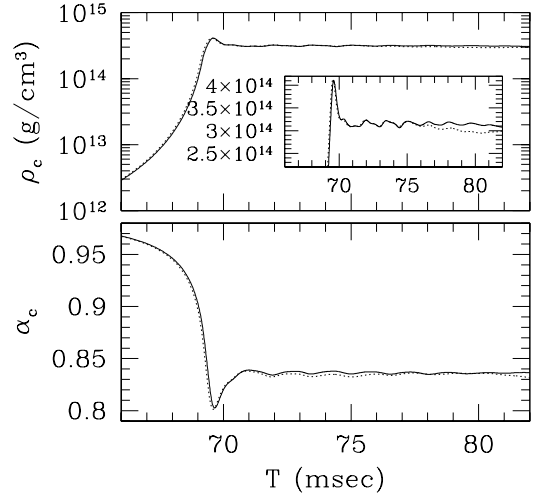
(a)



(b)

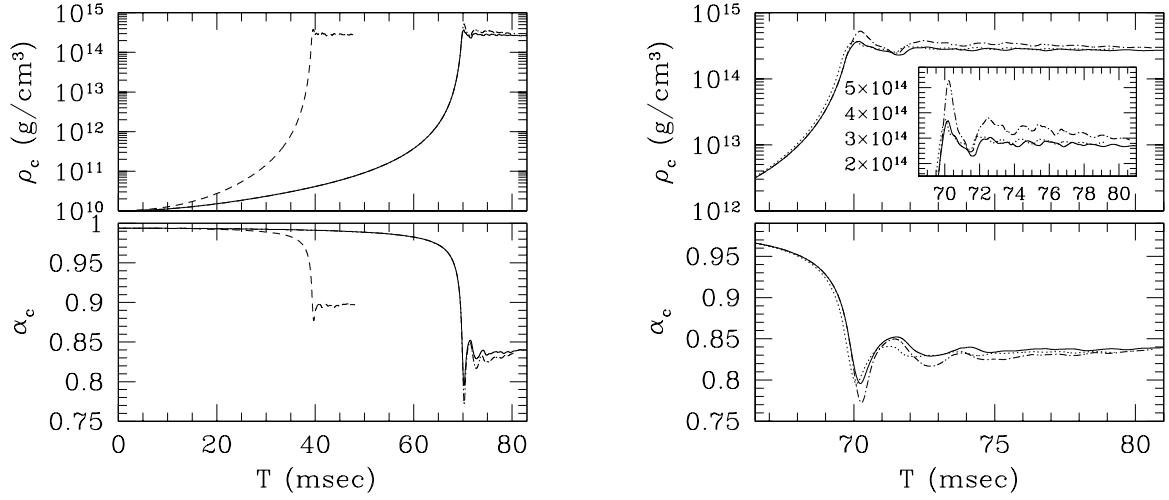


(c)

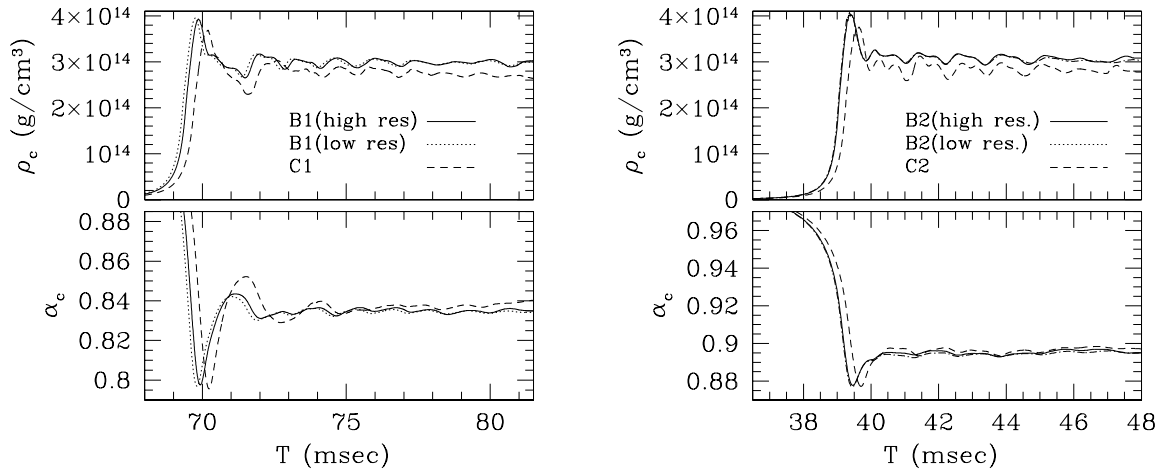


(d)

FIG. 1. Evolution of the central density and the central value of the lapse function for model A. (a) Models A1 (solid curve), A2 (dashed curve), and A3 (dotted-dashed curve); (b) Models A1 (solid curve), A4 (dotted curve), and A5 (dotted-dashed curve); (c) Models A1 (solid curve) and A6 (dotted curve); (d) Model A1 with high (solid curve) and low grid resolutions (dotted curve).



(a) (b)  
 FIG. 2. (a) The same as Fig. 1 but for models C1 (solid curves), C2 (dashed curves), and C3 (dotted-dashed curves). (b) The same as Fig. 1 but for models C1 (solid curves), C3 (dotted-dashed curves), and C4 (dotted curves).



(a) (b)  
 FIG. 3. (a) The same as Fig. 1 but for model B1 with high (solid curve) and low grid resolutions (dotted curve). For comparison, the results for model C1 (dashed curve) are also shown. (b) The same as (a) but for model B2 with high (solid curve) and low grid resolutions (dotted curve) and for model C2 (dashed curve).

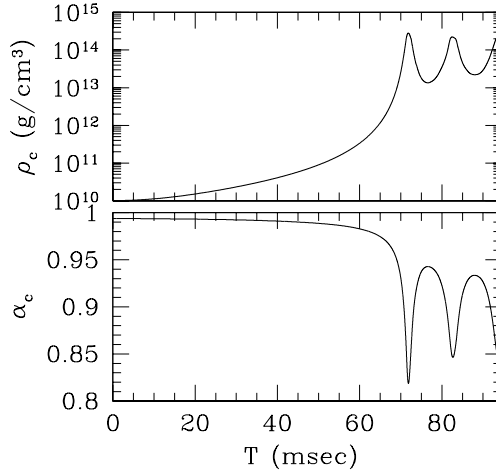


FIG. 4. Evolution of the central density and the central value of the lapse function for model D.

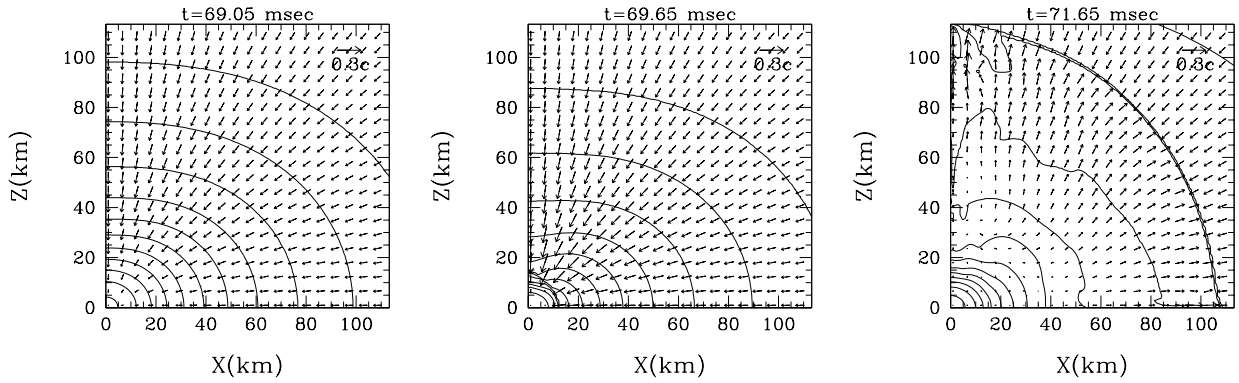


FIG. 5. Snapshots of the density contour curves of  $\rho$  and of the velocity field of  $(v^x, v^z)$  at selected time slices around which shocks are formed for model A1. The contour curves are drawn for  $\rho/\rho_{\text{nuc}} = 3 \times 10^{-0.4j}$ , with  $j = 0, 1, 2, \dots, 15$ .

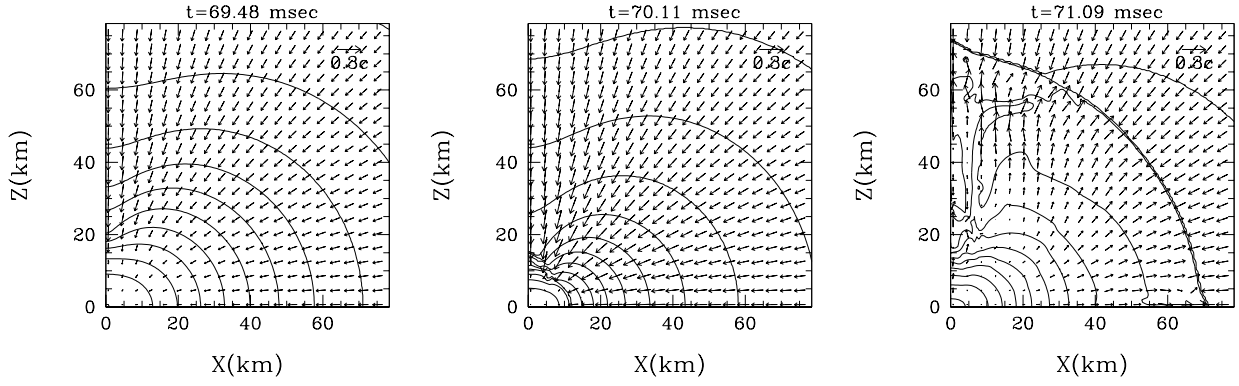
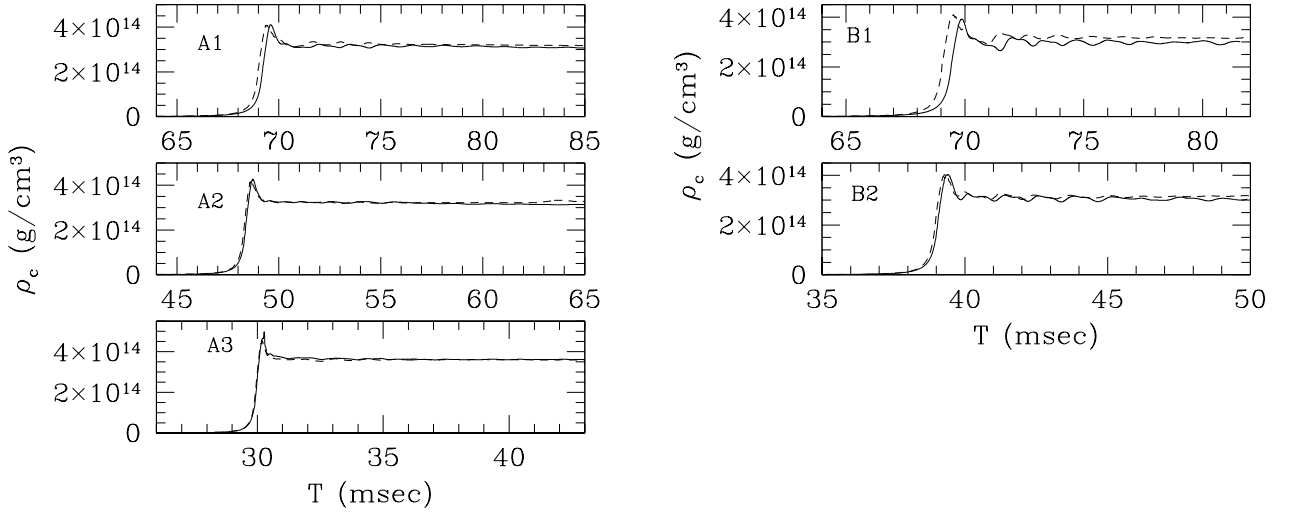
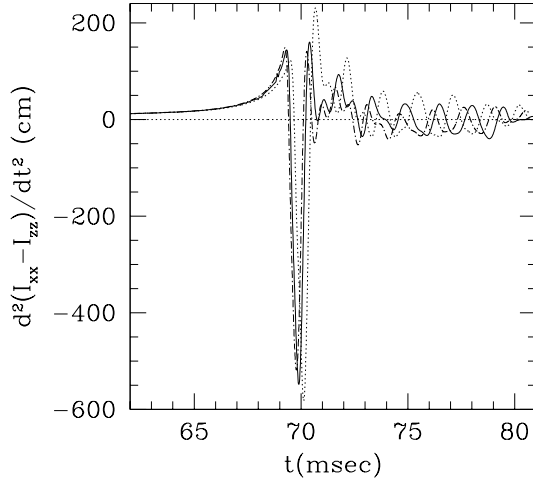


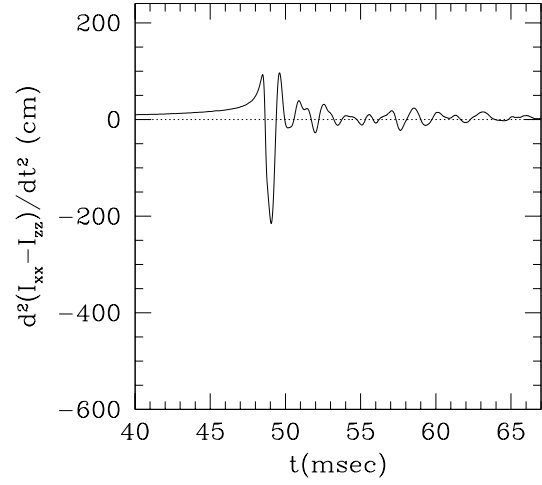
FIG. 6. The same as Fig. 5 but for model C1. The contour curves are drawn for  $\rho/\rho_{\text{nuc}} = 3 \times 10^{-0.4j}$ , with  $j = 0, 1, 2, \dots, 15$ .



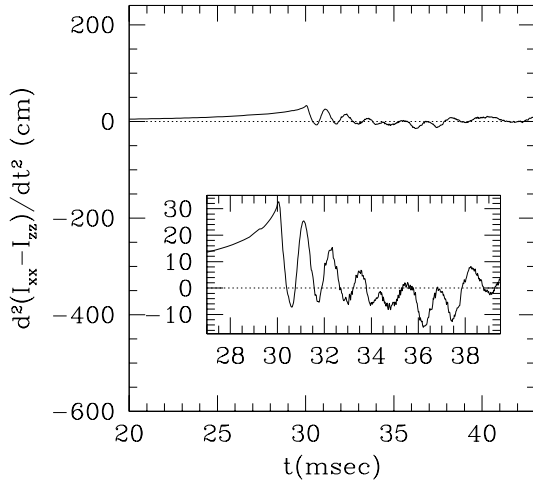
(a) (b)  
 FIG. 7. Comparison between the evolution of the central density computed in this paper (solid curves) and in Dimmelmeier et al. (dashed curves) (a) for models A1–A3 and (b) for models B1 and B2.



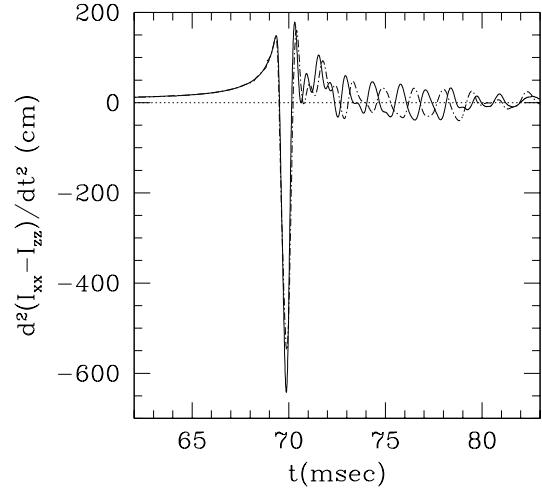
(a)



(b)

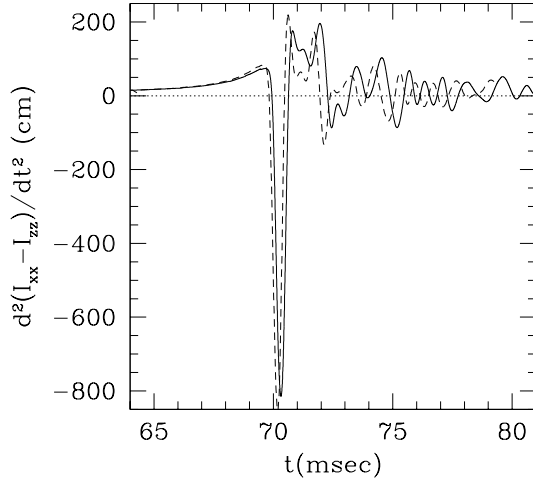


(c)

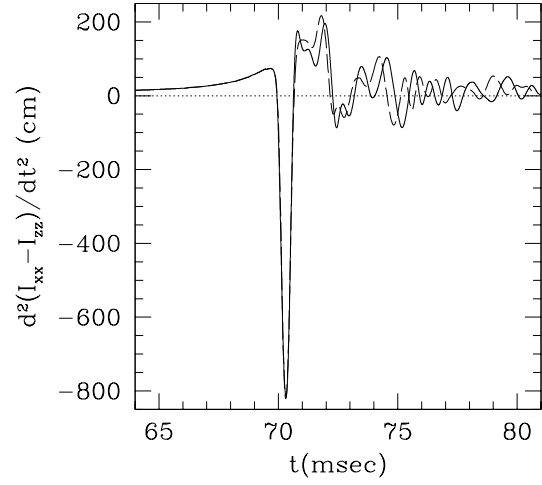


(d)

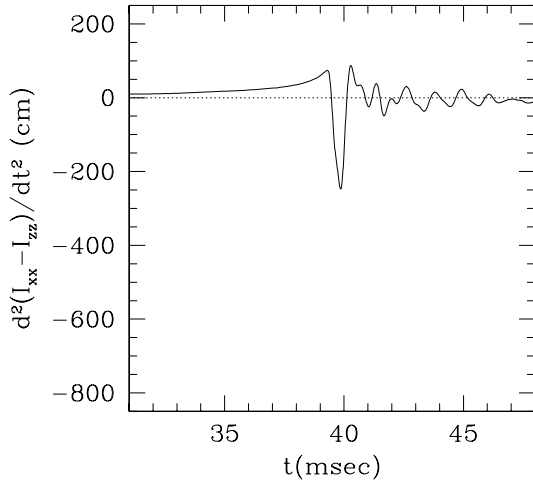
FIG. 8. Gravitational waveforms for model A; (a) Models A1 (solid curve), A4 (dotted-dashed curve), and A5 (dotted curve); (b) Model A2; (c) Model A3; (d) Models A6 (solid curve) and A1 (dashed curves) grid resolutions.



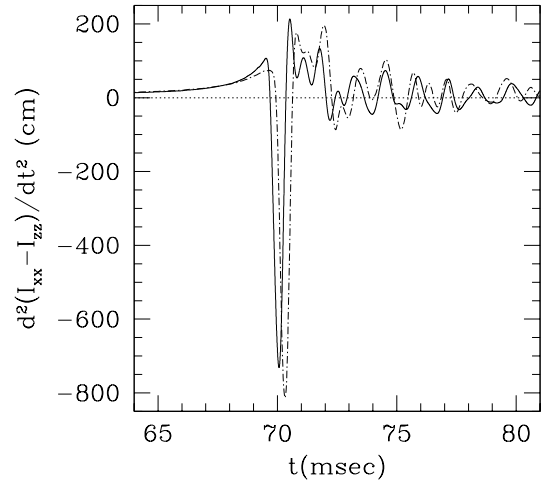
(a)



(b)



(c)



(d)

FIG. 9. Gravitational waveforms for model C; (a) Models C1 (solid curves) and C4 (dashed curves); (b) Models C1 (solid curves) and C3 (long-dashed curves); (c) Model C2; (d) Models B1 (solid curve) and C1 (dotted-dashed curve).

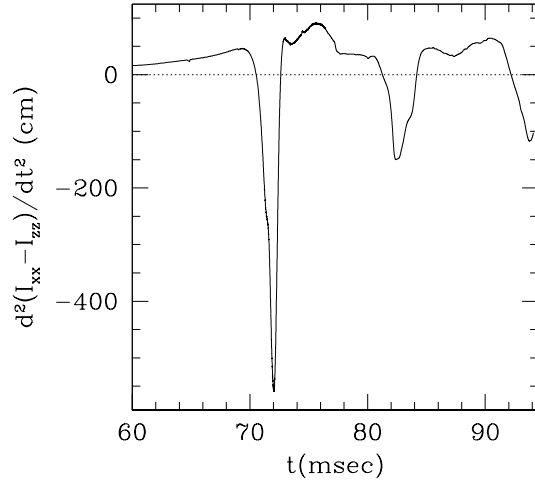


FIG. 10. Gravitational waveforms for model D.

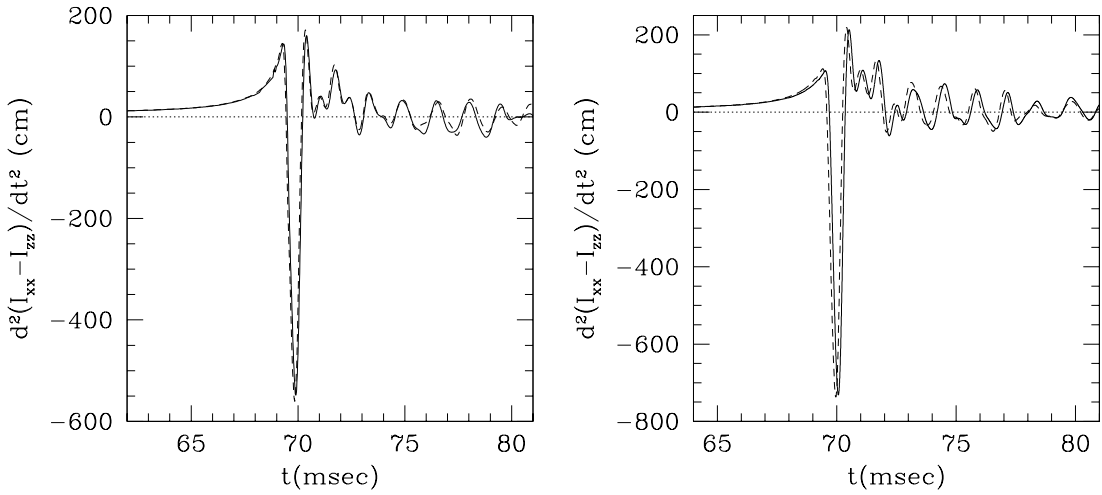
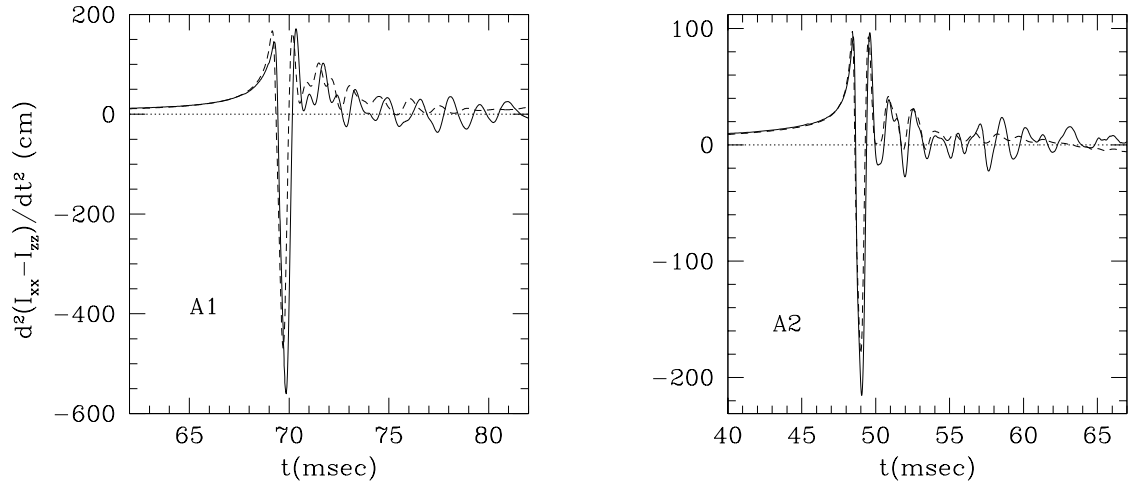


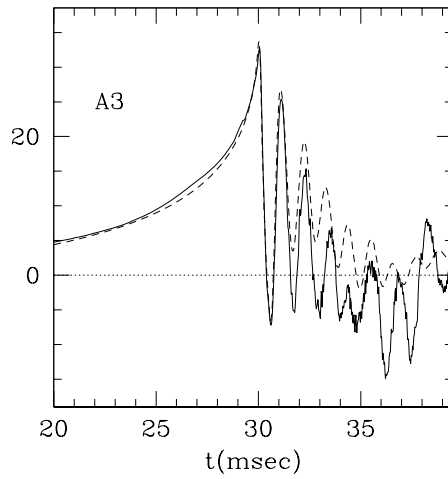
FIG. 11. Gravitational waveforms (a) for model A1 and (b) for model B1 with high (solid curve) and low grid resolutions (dashed curve).





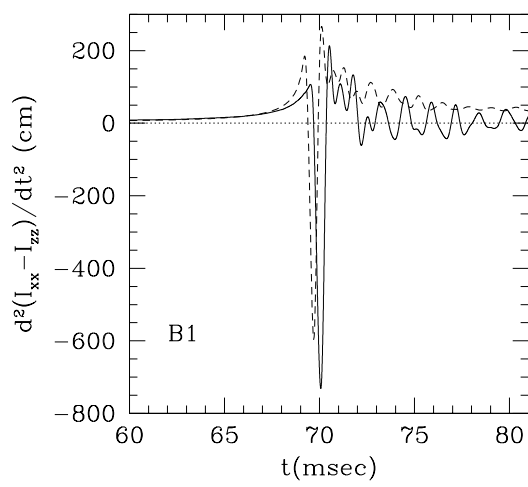
(a)

(b)

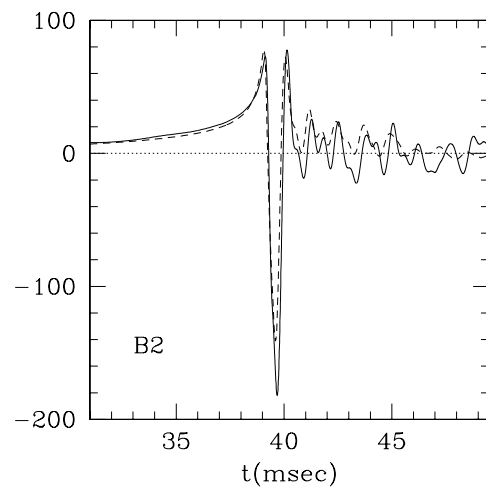


(c)

FIG. 12. Comparison between gravitational waveforms computed in this paper (solid curves) and in Dimmelmeier et al. (dashed curves) for models A1–A3 [(a)–(c)].



(a)



(b)

FIG. 13. The same as Fig. 12 but for models B1 and B2 [(a) and (b)].